

# A new methodological approach to evaluate the mass and volume distributions of grains in an agglutinated foraminiferal test

Eric Armynot du Châtelet<sup>1</sup>, Fabrizio Frontalini<sup>2</sup>, François Guillot<sup>1</sup>

<sup>1</sup>Université Lille 1, UMR 8217 CNRS Géosystèmes, UFR Sciences de la Terre,  
Bât SN5, 59655 Villeneuve d'Ascq cedex, France

<sup>2</sup>Dipartimento di Scienze della Terra, della Vita e dell'Ambiente (DiSTeVA), Università degli Studi di Urbino  
"Carlo Bo", Campus Scientifico Enrico Mattei, Località' Crocicchia, 61029 Urbino (Italy)  
email: Eric.Armynot@univ-lille1.fr

**ABSTRACT:** Chemical maps and images were made of the test of *Textularia earlandi*, an agglutinated foraminifera, by ESEM-EDS (Environmental Scanning Electron Microscopy-Energy Dispersive Spectrometer). The specimen is about 300µm long, comprising 17 imbricated growth chambers. In order to evaluate the mass distribution along the test, mineral grain densities, as deduced through chemical mapping, as well as the volumes of 650 grains, were treated by geostatistical methods. The volume of the imbricated spheres was 3D-modelled using the Monte-Carlo method. It is calculated that the volume of the chamber grows regularly. The mass of the chambers undergo some variation due to occurrence of various proportions of minerals with different densities. The mass distribution within each chamber is smoothly distributed. Further development on other protists with various shape and geometry could be easily imagined.

**Keywords:** agglutinated benthic foraminifera; volume; mass; geostatistics

## INTRODUCTION

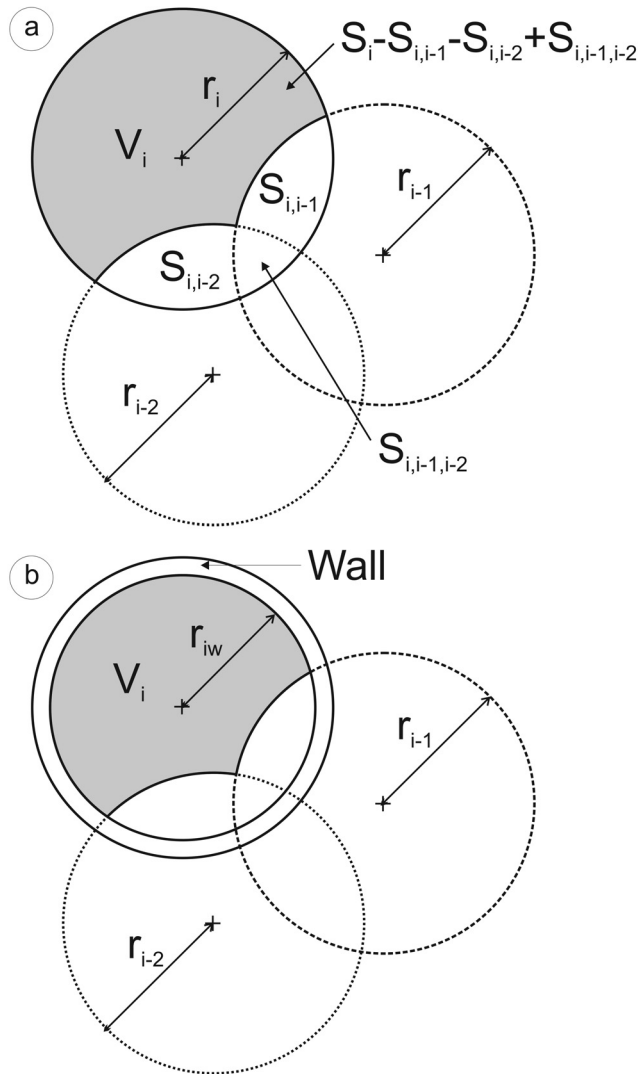
Foraminifera, which are single-celled organisms, are among the best known and the most diversified of all microfossils (Murray 2006). They are widely distributed in all marine and transitional marine environments (Scott et al. 2001), and play a significant role in global biogeochemical cycles of inorganic and organic compounds, making them one of the most diversified and studied groups on Earth (e.g., Haynes 1981, Lee and Anderson 1991). Foraminifera are protists that are an important part of the food web, but little or no attention has been paid to the ways in which they expend their energy.

Foraminifera tests are composed of either organic material, secreted CaCO<sub>3</sub>, or agglutinated foreign particles. The latter types of test, which are classified under the sub-class Textulariia (Loeblich and Tappan 1987), collect particles from the surrounding environment and agglutinate them onto an inner organic layer protecting the cell (Bender 1993, Bender 1992, Lipps 1973). The cement binding the grains together may be organic (as in the common and well known *Jadammina macrescens*, *Miliammina fusca*, or *Trochammina inflata*), calcitic (as in Textulariida; (Bender and Hemleben 1988), or of a mixed nature (as in Lituolida and Loftusiida, which contain organically-cemented, calcareous and microgranular types; (Kaminski 2004). Agglutinated foraminifera use a great variety of materials to produce their tests. Some show little or no selectivity, whereas others are very particular about the foreign matter they use (Lipps 1973, Norman 1878, Heron-Allen 1915, Armynot du Châtelet et al. 2013a, Armynot du Châtelet et al. 2008). Although our understanding of agglutinated foraminiferal ecology, distribution and classification has advanced in the last few decades, further studies are required to enhance our

knowledge of the mechanisms of grain selection (Bowser and Bernhard 1993, Bertram and Cowen 1998).

To understand this selectivity, grains should be accurately described in terms of all of their characteristics of size, mineralogy and mass. The size and mineral species of agglutinated grains are variable, and have already been investigated (Armynot du Châtelet et al. 2008, Makled and Langer 2010). Agglutinating characteristics have been used for the purposes of species classification (Hofker 1972, Hohenegger 1990). However, few studies have been published about their mass. Gooday and Cloughera (1989) investigated the distribution of grains in the test, and demonstrated that some Bathysyphon species (*B. capillare*) have a well-defined, outer layer consisting of flat-lying or imbricated plate-like mineral grains, whereas other species from the same genus (*B. rufus*) do not display any organization within the agglutinated grains. The peculiar distribution of the grains may affect their mass distribution. By the same token, Roth et al (2011) have suggested that the presence of intracellular high density barite grains is species specific. Moreover, Cole and Valentine (2006) observed the needle of TiO<sub>2</sub>, the distribution of which within the test is still not explained, but the species clearly needs it. Particle size, shape and mass distribution should necessarily have an impact on the equilibrium of the test with respect to the optimal displacement/settling upon the substrate where it lives and/or feeds. All of these studies are based on a very peculiar mineral shape and mineralogy.

The spatial distribution of the mass can be accurately described and analyzed by geostatistical methods, which are preferential to classical statistics that assume completely independent measurements. Geostatistics have rarely been applied to foram-



TEXT-FIGURE 1  
Basic schemes for volume calculation of 3 intersected spheres represented in 2D. a) is for external volume and b) is for internal volume taking into account the wall thickness.  $r$  are the different radii and  $V$  the volumes.

iniferal analyses (once by Armynot du Châtelet et al. 2012, who illustrated the spatial variability of foraminifera and associated biotas), and so herein we make a first attempt to describe the spatial variability at the test and chamber level, characterizing the agglutinated material in one foraminiferal test.

Biometric analysis is recognized as being of great value (Scott 1980), even if, with foraminifera, it is mainly used for classification purposes (Kaminski 1984). Most of the time, the numerical characterization of the morphological variability is based on chamber length and height (Georgescu and Almogi-Labin 2008). Biometry and the growth patterns of foraminifera are now largely facilitated with non-destructive techniques such as micro-CT scanning (Speijer et al. 2008, Briguglio et al. 2011).

Nevertheless, access to high quality facilities at a low price is still not democratized.

The objective of this research is to carry out an integrated study combining an investigation of the mineralogy and mass of the grains, focusing on their spatial distribution by using geostatistics. The two challenges of this study are to conduct the analyses on: (1) a ubiquitous, selected foraminiferal species (*Textularia earlandi*; Parker, 1952); and (2) classical ESEM pictures that can be modelled to both obtain the 3D shape of the foraminifera and estimate biometric parameters such as several volume and mass figures.

## MATERIAL AND METHODS

### Sample acquisition

Sediment samples were collected within the superficial, silty sediment of the Marmara Sea shelf (sample 3, as described in Chende? et al. 2004; Frontalini et al. 2011; and Armynot du Châtelet et al. (2013a)). One specimen of the agglutinated foraminiferal species *Textularia earlandi* Parker, 1952, was selected for the analyses. This species was chosen as it is widely distributed and can be described within contrasting environments such as a polluted harbour (Scott et al. 2005), the fjords of Baffin Bay, where it is dominant (Schafer and Cole 1988), or in mangroves (Javaux and Scott 2003). Phleger (1965), in his inventory of the living depth patterns of benthic foraminifera, reported that *Textularia earlandi* lives in subtidal environments with a shallow limit of 35–45m. Moreover, the cement binding the grains is of an organic matter composition, offering a sharp chemical contrast to mineral grain compositions, making grain by grain analysis easier than in other available species. Finally, this species organizes its agglutinated grains in a single layer, which is a key point with respect to the different assumptions developed in the present study.

### General morphology of *Textularia earlandi*

The wall of *Textularia earlandi* is agglutinated with medium to fine mineral grains and other particles. The test is minute, biserially arranged, very elongate straight or slightly curved, and oval in section. The chambers are very numerous, up to 12 or more pairs, following the initial stage, and distinct and slightly depressed. The shape of the chambers is sub-rounded, increasing in size as added. The sutures are very slightly depressed. The aperture is distinct and allows for an arch on the inner edge of the terminal chamber.

### ESEM-EDS image acquisition

The chemical determination of the agglutinated minerals within the test of the agglutinated foraminifera was carried out by way of elemental chemical mapping using an Environmental Scanning Electron Microscope (ESEM) equipped with an Energy-Dispersive Spectroscopy (EDS) device. This technique permits the user to work on natural, rough surfaces where polishing is not possible and 3D observation is necessary for species determination and the observation of grain shapes. The foraminiferal test was placed on a stub and then carbon-coated. This test was first pictured by using a secondary electron for the general shape, before being imaged for elemental mapping (Si, Al, Mg, Na, K, Ca, Ti and Fe) under low-vacuum conditions using a 20kV beam. The mineralogy of the foraminiferal test was also quantified using oxide proportions retrieved after a point analysis obtained with the ESEM-EDS. Mineral names were chosen after the point chemical analyses. Chemically coded col-

our imaging helped in separating the grains according to their chemical compositions, while conventional backscattered electron (BSE)-imaging assisted in localizing high-Z element-rich grains because of their stronger reflectivity.

#### Estimation of the volume of the chambers and the whole specimen

The calculations of the volume of each chamber and the global volume of the specimen were estimated in order to visualize the repartition of the mass throughout the specimen. Both the internal and external volumes (internal + wall thickness) were estimated using the classical Monte Carlo procedure. The Monte Carlo procedure is an estimation obtained by random sampling (up to 109 trials per measurement), where a stochastic model of rainfall is used to generate a long synthetic input series for the mathematical model.

We estimated that each chamber might be assimilated to a sphere. The centre coordinates ( $x, y, z$ ) and the radius ( $r$ ) were estimated visually from the SEM pictures. In the absence of 3D-information about the centre altitude ( $z$ ), it was provisionally supposed that all of the centres lie on the  $z = 0$  plane. For the purposes of generalizing the calculations that follow, the  $z$  parameter was taken into account hereafter.

The volume of chamber  $i$  (text-fig. 1) is given as Equation 1:

$$V_i = \frac{4}{3}\pi r_i^3 - S_{i,i-2} + S_{i,i-1,i-2} \quad (\text{Eq. 1})$$

where  $S_{i,i-1}$  and  $S_{i,i-2}$  are the common volumes of the interiors of the spheres  $i$ , ( $i-1$ ) and ( $i-2$ ).  $S_{i,i-1}$  and  $S_{i,i-2}$  are the volumes of the common interiors of the spheres  $i$ , ( $i-1$ ) and ( $i-2$ ) (text-fig. 1a).

$S_{i,i-1}$  and  $S_{i,i-2}$  were calculated using the textbook formula in Eq. 2:

$$S_{i,i-1} = \frac{\pi(R+r-d)^2(d^2 + 2dr - 3r^2 + 2dR + 6rR - 3R^2)}{12d} \quad (\text{Eq. 2})$$

Equation 2 is valid for  $d \leq R+r$ , and for two spheres of radii  $R$  and  $r$  with distance  $d$  between their centres;  $d$  is the Cartesian distance between the centres of spheres  $i$  and ( $i-1$ ) and is calculated as follows (Eq. 3):

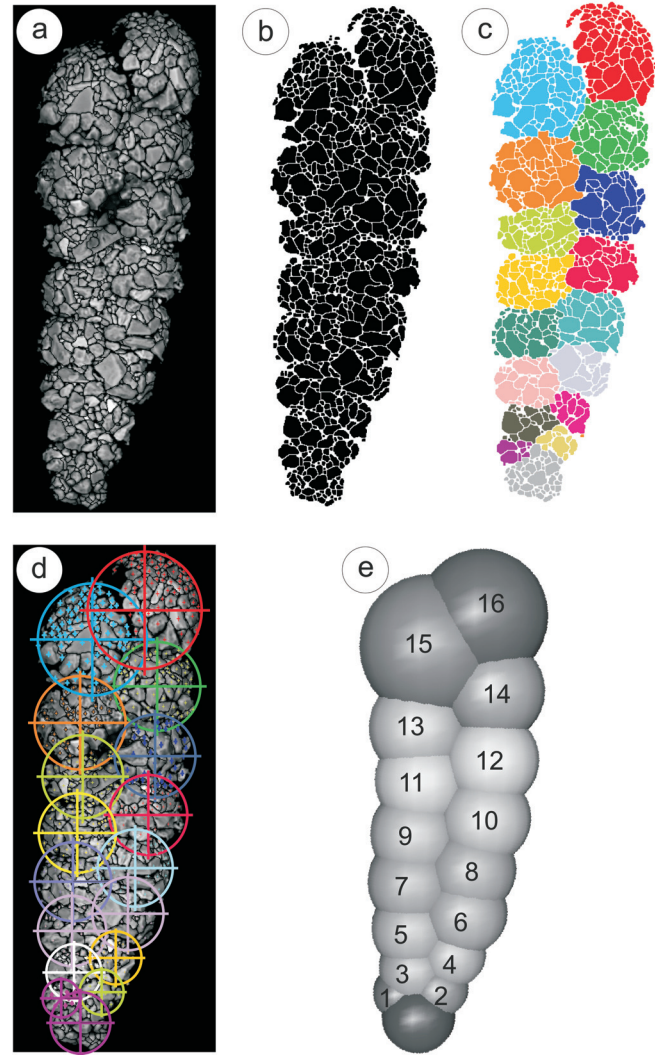
$$d = \sqrt{(x_i - x_{i-1})^2 + (y_i - y_{i-1})^2 + (z_i - z_{i-1})^2} \quad \text{Eq. 3}$$

A Monte-Carlo procedure was used to compute the volume  $V_{i,i-1,i-2}$  (the code in the R-language is given in Supplement 1, online). To calculate the internal volume of the chambers, the radius  $r_i$  of sphere  $i$  was diminished from the estimated wall thickness and became  $r_{iw}$  (text-fig. 1b). Growth models could then be calculated. All of these calculations were carried out using the R-software with the *base* and *lattice* packages.

#### Geostatistical analysis: spatial distribution of the mass of the grains

On the back-scattered image (text-fig. 2a), the grains were separated after the thresholding and watershed routines on the binary coded image using the image-J software (text-fig. 2b-c). The grains were then labelled and their characteristics were acquired. This included a measurement of their surface area and the position of their barycenter (text-fig. 2d).

As the shape of the chamber was not flat, the area of the grains was not initially properly evaluated. In former studies, the observed areas were selected to be as flat as possible, thereby reducing the number of analyzed grains (Armynot du Châtelet et



TEXT-FIGURE 2

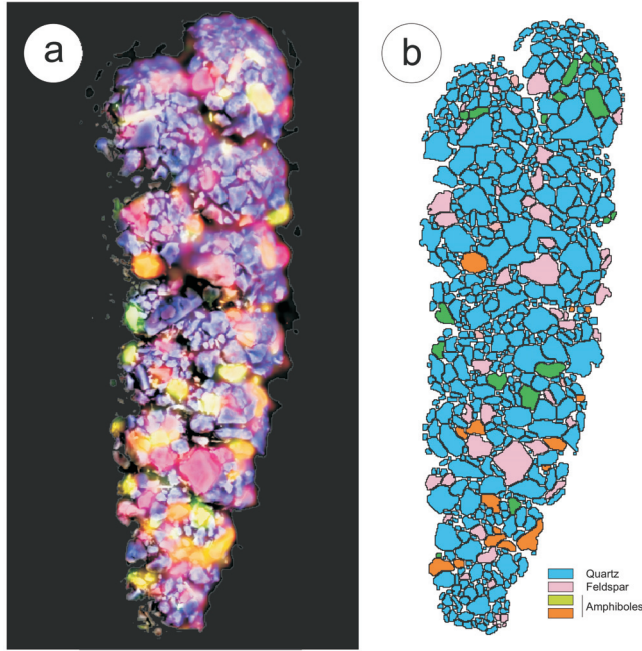
Image treatment study of agglutinated grains: a) SEM Back Scattered Electron picture (obtained in high vacuum at 25kV); b) BSE image after grey level threshold adjustment, binary conversion and watershed segmentation; c) Grain groupings according to the chambers; d) localization of the barycenter of the grains and center of the spheres bearing the grains; e) spherical modeling and labeling of the chambers.

al. 2013a, Armynot du Châtelet et al. 2010). Herein, we propose a spatial geometry transformation, which maximizes the number of grains taken into account. By considering the position on the BSE image of the barycenter of the grains designed as  $x$  and  $y$ , and by assuming the radius  $r$  of the sphere upon which all of the grains from each chamber were associated, we defined the Cartesian coordinates ( $X, Y, Z$ ) of the barycenter of the grains as in Eq.4

$$\left\{ \begin{array}{l} X = x \\ Y = y \\ Z = \sqrt{(r^2 - x^2 - y^2)} \end{array} \right\} \quad (\text{Eq. 4})$$

The resulting geometry could be visualized in a movie (Supplementary Material 2). The size of the grains and the equivalent





TEXT-FIGURE 3  
Method used for chemical analysis: a) combined color image from elemental analysis (detected elements were Si, Al, Mg, Na, K, Ca, Ti and Fe); b) interpretation of the mineralogy of the grains.

radius were then estimated after the recalculated area. On the one hand, by assuming that the wall was made of a single layer of grains, the medium diameter was estimated as the reliable thickness of the wall for the later calculation of the volume of the chambers. On the other hand, each mineral volume was then multiplied by its conventional density (quartz = 2.66, feldspar = 2.64, amphibole = 3.24) to obtain the mass.

The micro-distribution and spatial variability of mass within the specimen were described by way of a geostatistical analysis (Wackernagel 1988).

The Cartesian coordinates of the grains were first converted to spherical coordinates by using the following equations (Eq. 5):

$$\begin{aligned}\theta &= \tan^{-1} \left( \frac{\sqrt{x^2 + y^2}}{z} \right) \\ \varphi &= \tan^{-1} \left( \frac{y}{x} \right) \\ r &= r\end{aligned}\quad \text{Eq. 5}$$

$z$  is defined as the radius of the sphere carrying the grains.

The two defined angles with the spherical coordinates were then used for grain localization within the following calculation. After a log transformation for normality adjustment (Shapiro-Wilk test; (Shapiro 1965), a semivariogram for each chamber was calculated by Eq. 6:

$$\gamma(h) = \frac{1}{2n_h} \sum_{i=1}^{n_h} [Z(x_i + h) - Z(x_i)]^2 \quad \text{Eq. 6}$$

where  $g(h)$  is the semivariance at lag distance  $h$  (in terms of  $\theta$  and  $\varphi$ ),  $n(h)$  is the number of observation pairs separated by  $h$ , and  $Z(x_i)$  and  $Z(x_i + h)$  represent the paired values of variable  $Z$  in two locations separated by  $h$ . The semivariogram can be fitted by using numerous models. The present study considers cubic, spherical, Gaussian and linear models (respectively, equations 7 to 10), which were commonly mixed with a nugget model (Eq. 11). The nugget represents the variability at distances smaller than the fixed sample spacing, including measurement error.

Cubic model:

$$\gamma(h) = \begin{cases} C(7r^2 - 8.75r^3 + 3.5r^5 - 0.75r^7) & \text{if } r < 1; \text{ with } r = \frac{h}{a} \\ C & \text{otherwise} \end{cases} \quad \text{Eq. 7}$$

Spherical model:

$$\gamma(h) = \begin{cases} C \left( 1.5 \left( \frac{h}{a} \right) - 0.5 \left( \frac{h}{a} \right)^3 \right) & \text{if } h \leq a \\ C & \text{otherwise} \end{cases} \quad \text{Eq. 8}$$

$$\text{Gaussian model: } \gamma(h) = C \left( 1 - \exp \left( -\left( \frac{h}{a} \right)^2 \right) \right) \quad \text{Eq. 9}$$

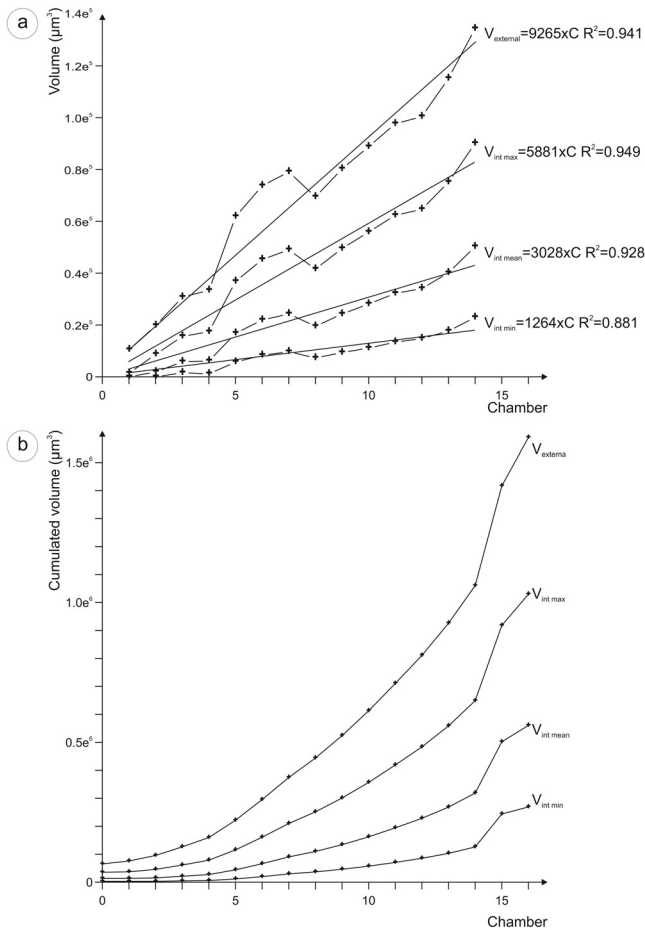
$$\text{Linear model: } \gamma(h) = C \times h^b \text{ (Power model with } b=1) \quad \text{Eq. 10}$$

$$\text{Nugget: } \gamma(h) = \begin{cases} 0 & \text{if } h = a \\ C & \text{otherwise} \end{cases} \quad \text{Eq. 11}$$

These equations use  $h$ ,  $a$  and  $C$  to represent the lag distance, the practical range and the sill, respectively. In the analysis, the sill value is the upper limit of the semivariogram model. As a consequence, the ratio of nugget to sill indicates the spatial dependency of the mass distribution (Webster and Oliver 2001, Webster 1990). The ratios were categorized as low (<25%), moderate (25 to 75%) or strong (>75%). A low ratio means that a large part of the mass variance is introduced spatially, implying the strong spatial dependency of the mass of the grains. A high ratio often indicates a weak spatial dependency. The range of the semivariogram represents the average distance through which the variable semivariance reaches its peak value (Weindorf and Zhu 2010). A small effective range implies a distribution pattern composed of small patches. Geostatistical analysis was carried out using the geoR package for the R software.

## RESULTS AND DISCUSSION

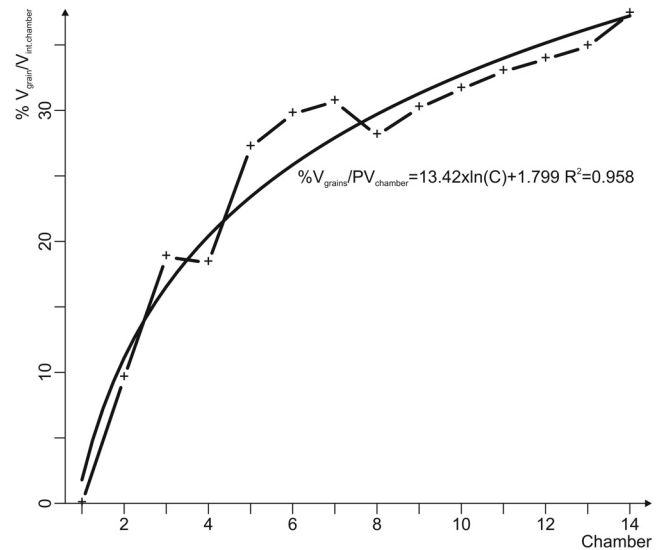
The specimen is comprised of a poorly defined proloculus (chamber labelled as 0), followed by 16 chambers distributed along two diverging axes. As we assumed that the test wall consists of a single layer of grains, all of the grains on the exposed side of the test are visible. A total of 652 grains are positioned, 605 of which do not consider the proloculus (text-fig. 2). The



TEXT-FIGURE 4  
Individual chamber volumes (a) and cumulated chamber volumes (b) of the studied specimen. Linear equations are added as growth model.

mineralogy is dominated by quartz (573 grains), followed by feldspar (48) and amphiboles (31) (text-fig 3). The number of analyzed grains per visible half chamber was between 8 (chamber labelled as 1) and 85 (chamber 15) (Table 1). The estimated mass of the half chamber (the observable part) increased from the proloculus to the last chamber, with variations such as in chamber 13, which is the heaviest, or chambers 11 and 14, which have lower masses than their closest neighbours (Table 1). The global mass pattern can be explained by the increasing chamber dimensions. The local pattern, meanwhile, may be described in terms of the variations in the number of grains with the lowest (very few amphiboles in chambers 14 and 11) or highest density (a high number of amphiboles in chamber 13).

The chamber volumes grow following a linear law (text-fig. 4a). As a consequence, the global volume of the specimen follows a power law (text-fig. 4b). The global volume was estimated to be  $1,589,341 \pm 42 \mu\text{m}^3$  (Table 1). On the basis of these results, the computing error is negligible compared to much greater expectable errors related to the shape parameter measurements and shape hypotheses. The proportion of the grains relative to the global volume of the chamber is best approximated by a logarithmic law (text-fig. 5). The distribution of the



TEXT-FIGURE 5  
Ratio between the volume of the grains compared to the volume of the internal part of the specimen (i.e. maximum available volume for the cell) along the chambers.

weight between the heavy wall and the light cell would thus be under some kind of control and probably tends towards an equilibrium. Even though the number of chambers could increase infinitely, as the wall is composed of a single layer of grains, the growth is probably limited by the strength of the associated grain-cement. These ideas support the notion that there is bioadhesive cement in this test structure (Bender 1993), (Bowser and Bernhard 1993)

We are currently considering a more detailed 3D investigation of the organization of the grains within the organic matrix using specimens with more contrasted agglutinated grains and X-ray microtomography. This investigation may help us to understand the test strength and growth limits. Even if such methods were used on the general morphological shape of foraminifera (Speijer et al. 2008), and with some additional measurements (Briguglio et al. 2011), to our knowledge, except our work on agglutinated testate amoebae (Armynot du Châtelet et al. 2013b), no experiments have been carried out on any agglutinated forms of protist.

From our geostatistical investigation (Table 2), the spatial dependency of mass distribution is weak to moderate for chambers 2 to 16 and strong for chamber 1. As the number of visible grains in chambers 1, 2 and 4 is very small, the results should be considered with caution. When spatial dependency is weak or moderate, the mass distribution is reputedly distributed randomly. The proportion of the nugget is always very high compared to the real mass variation around the chambers. The nugget model effect corresponds to a purely random phenomenon (with noise) with no correlation between values.

The models used are: cubic in the disputable case of chamber 1; spherical for chamber 15; and linear or Gaussian for the rest of the chambers. For the chambers where a Gaussian model is calculated, there is an extremely continuous phenomenon. This

TABLE 1

Chambers characteristics. Position of the center of the associated sphere (X, Y), radius (r), volume (ext = external intmax = higher possible internal volume, intmin = lowest possible internal volume, intmean = medium possible internal volume), number of analyzed grains for positioning (Nb), mass of the chamber.

Chamber	X	Y	r	Vext	Vintmax	Vintmin	Vintmean	Nb	Mass (g)
0	42.9	15.6	25.0	65302.6159	35621.2978	3198.0901	13512.1175	46	-
1	30.1	30.7	18.0	10498.142	1409.4342	0	0	8	5.003E-09
2	56.6	34.8	20.0	19795.589	8701.08056	0	1898.32406	10	5.919E-09
3	39.3	47.6	23.4	30748.2223	15611.9792	1562.21863	5784.82882	20	1.341E-08
4	65.8	57.8	22.4	33392.7806	17383.6471	1160.89702	6134.99435	12	9.355E-09
5	38.4	74.5	27.5	61843.5969	36825.8288	5683.93411	16812.291	31	2.442E-08
6	73.5	86.0	28.8	73719.9054	45257.6193	8302.0377	21914.6482	21	2.681E-08
7	38.4	105.6	30.1	79087.3317	49010.1516	9683.63325	24259.6272	35	2.223E-08
8	78.1	114.7	29.9	69437.876	41581.9619	7259.57656	19502.5742	33	3.034E-08
9	40.7	137.6	30.6	80221.2814	49491.8607	9363.17985	24222.9736	49	2.411E-08
10	86.8	148.5	30.7	88810.2512	55866.4008	11076.8805	28090.9285	30	3.989E-08
11	44.8	173.2	31.7	97668.8512	62328.517	13383.6597	32198.2291	51	2.257E-08
12	90.9	186.9	31.7	100415.616	64642.1746	14752.9284	34047.138	36	4.606E-08
13	42.9	207.9	33.7	115163.031	75130.4007	17660.0791	40164.8537	50	6.341E-08
14	92.3	231.6	33.7	134351.018	90086.0905	22919.4863	50199.4914	61	3.232E-08
15	50.7	260.4	47.3	356496.443	269119.691	117699.075	183129.174	85	5.653E-08
16	84.5	280.1	43.2	172388.643	111683.116	25427.4731	58859.7821	73	5.698E-08

means that the mass distribution is smooth. Mass distribution is a little rougher in the linear model, but both geostatistical models suggest that the mass along the chambers is continuously distributed. No very short range variation is detected, meaning that no area has a heavier (e.g. accumulation of amphiboles) or a lighter mass (e.g. accumulation of feldspar). In other words, the mass of the grains is regularly distributed along the specimen. For the mass distribution of the grains of chamber 15, the best fit to the spherical model suggests a gradual increase of the semivariance as a function of the distance between grain barycenters, implying that the mass is slightly more chaotically distributed.

We evaluated the mass distribution within the test. A few studies focus on the mass of the foraminiferal specimens and when it is given as a global mass of the test. As an example, Widbom (1984) measured the dry mass of specimens that were separated as calcareous or agglutinated tests. The evaluation of the individual mass and volume of the chamber and their constitutive grains is a step forward when it comes to comprehending the construction of the foraminiferal tests with agglutinated materials.

The current results show that it is likely that not only the shape (as concluded by Tuckwell et al. 1999), but also the mass, might be somehow taken into account before agglutinating the grain to the new chamber. By the same token, Roth et al. (2011) propose that the presence of heavy particles is species specific and suggests that species are able to discriminate between different kinds of particle. This selectivity of heavy particles should have an impact on the equilibrium of the specimen. Moreover, Cole and Valentine (2006) observed the needle of  $\text{TiO}_2$ , whose distribution within the test is still not explained, although the species clearly need it. In the present study, whatever the process, the mass is distributed as homogeneously as it is possible to detect. This indisputably renders the test equilibrated.

## CONCLUSION

The ESEM-EDS technique is suitable for acquiring simultaneously the grain shape and position, as well as the chemical nature, of the grains of the test of *Textularia earlandi*. Based on shape modelling, we have shown that the volume and the mass of the distribution of the chambers can be simultaneously evaluated. The volume is increasing linearly, and it is also possible to evaluate the mass distribution within each chamber. We concluded that this mass is smoothly distributed. The developed technique is limited to foraminifera whose chamber geometry is close to a sphere. Further developments on other foraminifera shapes and geometries can be imagined.

## ACKNOWLEDGMENTS

The authors acknowledge M. A. Kaminski for providing the samples and F. Goujon for the first calculation of the volume of the studied specimen, Philippe Recourt for his great ESEM-EDS mastery. The helpful comments and suggestions of the three anonymous reviewers are also gratefully acknowledged.

## SUPPLEMENTARY MATERIAL ONLINE

Supplement 1 - R programming language routine for volume estimation of the common part of 3 chambers assimilated as spheres.

Supplement 2 - Movie showing the position of the grain barycenters for chambers 1 to 16.

## REFERENCES

- ARMYNOT DU CHÂTELET, E., BOUT-ROUMAZEILLES, V., COCCIONI, R., FRONTALINI, F., GUILLOT, F., KAMINSKI, M. A., RE COURT, P., RIBOULLEAU, A., TRENTESAUX, A., TRIBOVILLARD, N. and VENTALON, S. 2013. Environmental control on shell structure and composition of agglutinated foraminifera along a proximal-distal transect in the Marmara Sea. *Marine Geology*, 335: 114–128.



TABLE 2

Semivariogram models for mass distribution of the grains. A log transformation is applied to data in order to limit numerical bias. Results of the Shapiro Wilk test are given as W. Normality is rejected when p-value <0.05. Used models are cubic (cub), gaussian (gau), linear (lin) and spherical (sph).

Chamber	Nb grains	Log transform	Shapiro test (W)	p-value	Model	C0	Range	C	C0/(C+C0)	Spatial dependency
1	8	yes	0.939	0.604	cub	1.0	1980.14	22401.97	0.00	strong
2	10	yes	0.925	0.398	lin	4.0	inf	0.00	1.00	weak
3	20	yes	0.958	0.500	lin	2.9	1.90	0.09	0.97	weak
4	12	yes	0.947	0.598	gau	1.0	2.07	1.36	0.42	moderate
5	31	yes	0.947	0.125	gau	4.0	4.93	0.34	0.92	weak
6	21	yes	0.929	0.132	lin	5.0	inf	0.11	0.98	weak
7	35	yes	0.971	0.478	lin	2.8	inf	0.00	1.00	weak
8	33	yes	0.967	0.410	lin	2.5	inf	0.02	0.99	weak
9	49	yes	0.960	0.096	gau	2.1	2.80	0.42	0.83	weak
10	30	yes	0.945	0.127	lin	3.8	inf	0.00	1.00	weak
11	51	yes	0.978	0.439	gau	2.7	6.93	0.28	0.91	weak
12	36	yes	0.960	0.216	gau	2.4	2.92	0.69	0.78	weak
13	50	yes	0.939	0.012	lin	3.6	inf	0.06	0.98	weak
14	61	yes	0.964	0.067	lin	2.7	inf	0.00	1.00	weak
15	85	yes	0.982	0.287	sph	1.7	2.77	0.72	0.70	moderate
16	73	yes	0.987	0.626	gau	2.0	14.40	2.04	0.49	moderate

ARMYNOT DU CHÂTELET, E., GUILLOT, F., RECOURT, P., VENTALON, S. and TRIBOVILLARD, N. 2010. Influence of sediment grain size and mineralogy on testate amoebae test construction. *Comptes Rendus Geoscience*, 342: 710–717.

ARMYNOT DU CHÂTELET, E., NOIRIEL, C. and DELAINE, M. 2013b. 3D morphological and mineralogical characterisation of testate amoebae. *Microscopy and Microanalysis*, 19: 1–12.

ARMYNOT DU CHATELET, E., RECOURT, P. and CHOPIN, V. 2008. Mineralogy of agglutinated benthic foraminifera; implications for paleo-environmental reconstructions. *Bulletin de la société géologique de France*, 179: 583–593.

BENDER, H. 1992. Chamber formation and biomineralization in *Textularia candeiana* d'Orbigny (Sarcodina: Textularia). *Journal of Foraminifera Research*, 22: 229–241.

———, 1993. Test structure and classification in agglutinated foraminifera. In: Kaminski, M. A., Geroch, S. and Gasinski, M. A., Eds., *Proceedings of the fourth international workshop on agglutinated foraminifera*, 27–70. Krakow: Grzybowski Foundation. Special Publication 4.

BENDER, H. and HEMLEBEN, C., 1988. Constructional aspects in test foramination of some agglutinated foraminifera. In: Gradstein, F. M. and Rögl, F., Eds., *Second Workshop on Agglutinated Foraminifera*, 13–21. Vienna: Abhandlungen der Geologischen Bundesanstalt, 41.

BERTRAM, M. A. and COWEN, J. P. 1998. Biomineralization in agglutinating foraminifera: An analytical SEM investigation of external wall composition in three small test forms. *Aquatic Geochemistry*, 4: 455–468.

BOWSER, S. S. and BERNHARD, J. M. 1993. Structure, bioadhesive, and elastic properties of the agglutinated test of *Astrammina rara*. *Journal of Eukaryotic Microbiology*, 40: 121–131.

BRIGUGLIO, A., METSCHER, B. and HOHENEGGER, J. 2011. Growth rate biometric quantification by X-ray microtomography on larger benthic foraminifera: Three-dimensional measurements push nummulitids into the fourth dimension. *Turkish Journal of Earth Sciences*, 20: 683–699.

COLE, K. and VALENTINE, M. 2006. Titanium biomaterials: titania needles in the test of the foraminiferan *Bathysiphon argenteus*. *Dalton Transactions*, 2006: 430–432.

GEORGESCU, D. M. and ALMOGI-LABIN, A. 2008. New data to support the phylogenetic relationship between the serial planktonic foraminifera (Family Heterohelidae Cushman, 1927) and some large-sized benthic foraminifera (Family Orbitoididae Schwager, 1876) of the Late Cretaceous. *Revue de Paléobiologie*, 27: 15–24.

GOODAY, A. J. and CLAUGHERA, D. 1989. The genus *Bathysiphon* (Protista, Foraminiferida) in the northeast Atlantic: SEM observations on the wall structure of seven species. *Journal of Natural History*, 23: 591–611.

HAYNES, J. R., 1981. *Foraminifera*. New York: John Wiley and Sons, 433pp.

HERON-ALLEN, E. 1915. A short statement upon the theory, and the phenomena of purpose and intelligence exhibited by the Protozoa, as illustrated by selection and behaviour in the Foraminifera. *Journal of the Royal Microscopical Society*, 1915: 547–557.

HOFKER, J. S., 1972. *Primitive agglutinated foraminifera*. Leiden: EJ Brill, 95pp.

HOHENEGGER, J., 1990. On the way to optimal suprageneric classification of agglutinating foraminifera. In: Hemleben, C., Kaminski, M. A., Kuhnt, W. and Scott, D. B., Eds., *Paleoecology, biostratigraphy, paleoceanography and taxonomy of agglutinated foraminifera*, 77–104. NATO ASI Series C, vol. 327. Dordrecht: Kluwer Academic Publishers.

JAVAUX, E. J. and SCOTT, D. B. 2003. Illustration of modern benthic foraminifera from Bermuda and remarks on distribution in other subtropical/tropical areas. *Palaeontologia electronica*, 6: 1–29.

KAMINSKI, M. A. 1984. Shape variation in *Spiroplectammina spectabilis* (Grzybowski). *Paleontologia*, 29: 229–249.

———, 2004. *The year 2000 classification of the agglutinated foraminifera*. In: Bubik, M. K. and Kaminski, M. A., Eds. *Proceedings of the Sixth International Workshop on Agglutinated Foraminifera*, 237–255. Krakow: Grzybowski Foundation. Special Publication 8.

LEE, J. J. and ANDERSON, O. R., 1991. *Biology of foraminifera*. New York: Academic Press.

LIPPS, J. H. 1973. Test structure in foraminifera. *Annual Review of Microbiology*, 27: 471–488.

- LOEBLICH, A. R. and TAPPAN, H., 1987. *Foraminiferal genera and their classification*. New York: Van Nostrand Reinhold Co., 2 vols., 970 pp., 847 pls.
- MAKLED, W. A. and LANGER, M. R. 2010. Preferential selection of titanium-bearing minerals in agglutinated Foraminifera: Ilmenite (FeTiO<sub>3</sub>) in *Textularia haueri* d'Orbigny from the Bazaruto Archipelago, Mozambique. *Revue de Micropaleontologie*, 53: 163–173.
- MURRAY, J. W., 2006. *Ecology and applications of benthic foraminifera*. Cambridge: Cambridge University Press, 426pp.
- NORMAN, M. A. 1878. On the architectural achievement of little masons, annelidan (?) and rhizopodan, in the abyss of the Atlantic. *Annals and Magazine of Natural History*, 5: 284–288.
- PHLEGER, F. B. 1965. Depth patterns of benthonic foraminifera in the eastern Pacific. *Progress in Oceanography*, 3: 273–287.
- ROTHER, N., GOODAY, A. J. and PEARCE, R. B. 2011. Intracellular mineral grains in the xenophyophore *Nazareammina tenera* (Rhizaria, Foraminifera) from the Nazaré Canyon (Portuguese margin, NE Atlantic). *Deep Sea Research Part I: Oceanographic Research Papers*, 58: 1189–1195.
- SCHAFER, C. T. and COLE, F. E. 1988. Environmental associations of Baffin Island fjord agglutinated foraminifera. *Abhandlungen der Geologischen Bundesanstalt*, 41: 307–323.
- SCOTT, D. B., MEDIOLI, F. S. and SCHAFER, C. T., 2001. *Monitoring in coastal environments using foraminifera and thecamoebian indicators*. Cambridge: Cambridge University Press, 177.
- SCOTT, D. B., TOBIN, R., WILLIAMSON, M., MEDIOLI, F. S., LATIMER, J. S., BOOTHMAN, W. A., ASIOLI, A. and HAURY, V. 2005. Pollution monitoring in two north american estuaries: historical reconstructions using benthic foraminifera. *Journal of Foraminifera Research*, 35: 65–82.
- SCOTT, G. H. 1980. The value of outline processing in the biometry and systematics of fossils. *Palaeontology*, 23: 757–768.
- SHAPIRO, S. S. 1965. An analysis of variance test for normality (complete samples). *Biometrika*, 52: 591–611.
- SPEIJER, R. P., VAN LOO, D., MASSCHAELE, B., VLASSEN-BROECK, J., CNUDE, V. and JACOBS, P. 2008. Quantifying foraminiferal growth with high-resolution X-ray computed tomography: New opportunities in foraminiferal ontogeny, phylogeny, and paleoceanographic applications. *Geosphere*, 4: 760–763.
- TUCKWELL, G. W., ALLEN, K., ROBERTS, S. and MURRAY, J. W. 1999. Simple models of agglutinated foraminifera test construction. *Journal of Eukaryotic Microbiology*, 46: 248–253.
- WACKERNAGEL, H., 1988. Geostatistical techniques for interpreting multivariate spatial information. In: Chung, C. F. E. A., Ed., *Quantitative analysis of mineral and energy resources*, NATO ASI. Dordrecht: Reidel.
- WEBSTER, R. and OLIVER, M. A., 1990. *Statistical methods in soil and land resource survey*. Oxford: Oxford University Press.
- , 2001. *Geostatistics for environmental scientists*, Chichester: John Wiley & Sons.
- WEINDORF, D. C. and ZHU, Y. 2010. Spatial variability of soil properties at Capulin volcano, New Mexico, USA: Implications for sampling strategy. *Pedosphere*, 20: 185–197.
- WIDBOM, B. 1984. Determination of average individual dry weights and ash-free dry weights in different sieve fractions of marine meiofauna. *Marine Biology*, 84: 101–108.